Wind and Structures, *Vol. 25, No. 2 (2017) 157-176*
DOI: https://doi.org/10.12989/was.2017.25.2.157

Effect of beam slope on the static aerodynamic response of edge-girder bridge-deck

Hoyeop Lee[1a], Jiho Moon[2b], Nakhyun Chun[1c] and Hak-eun Lee[*1]

[1]*School of Civil, Environmental and Architectural Engineering, Korea University, Seoul 02841, South Korea*
[2]*Department of Civil Engineering, Kangwon National University, Chuncheon-si, Gangwon-do 24341, South Korea*

(Received January 13, 2017, Revised June 27, 2017, Accepted July 10, 2017)

Abstract. 2-edge box girder bridges have been widely used in civil engineering practice. However, these bridges show weakness in aerodynamic stability. To overcome this weakness, additional attachments, such as fairing and flap, are usually used. These additional attachments can increase the cost and decrease the constructability. Some previous researchers suggested an aerodynamically stabilized 2-edge box girder section, giving a slope to the edge box instead of installing additional attachments. However, their studies are limited to only dynamic stability, even though static aerodynamic coefficients are as important as dynamic stability. In this study, focus was given to the evaluation of static aerodynamic response for a stabilized 2-edge box girder section. For this, the slopes of the edge box were varied from 0° to 17° and static coefficients were obtained through a series of wind tunnel tests. The results were then compared with those from computational fluid dynamics (CFD) analysis. From the results, it was found that the drag coefficients generally decreased with the increasing box slope angle, except for the specific box slope range. This range of box slope varied depending on the B/H ratio, and this should be avoided for the practical design of such a bridge, since it results in poor static aerodynamic response.

Keywords: static aerodynamic response; 2-edge box-girder bridge; wind tunnel test; CFD analysis

1. Introduction

The 2-edge box girder section, shown in Fig. 1, has been widely used for various civil engineering practices including stiffened girder for the long span cable-stayed bridge, since it has good constructability and is cost effective (Simiu and Scanlan 1996, Matsumoto *et al.* 2000). However, it is known that the 2-edge box girder section has weak aerodynamic stability, including a high aerodynamic static coefficient, high vortex-induced vibration (VIV), and low flutter speed, compared to the single box girder section (Ito 1996, Miyata 2003).

Several studies have been conducted to improve the aerodynamic stability of the bridge section.

*Corresponding author, Professor, E-mail: helee@korea.ac.kr
[a] Ph.D. Student, Email: yopye@korea.ac.kr
[b] Assistant Professor, Email: jmoon1979@kangwon.ac.kr
[c] Ph.D. Student, Email: nhchun84@gmail.com

http://www.techno-press.org/?journal=was&subpage=8 ISSN: 1226-6116 (Print), 1598-6225 (Online)

The flap and fairing are often used to improve the aerodynamic stability of the bridge section (Bruno *et al.* 2001). Haque *et al.* (2016) investigated the effect of fairing shape on the aerodynamic stability of the bridge section by using computational fluid dynamics (CFD). Matsumoto *et al.* (2001) studied the effect of the grating on the flutter stability through a series of wind tunnel tests. Sakai *et al.* (1993) investigated the effect of various attachments, such as fairing, flap, edge plate, side plate, and baffle plate, to improve the aerodynamic stability of the edge girder section.

All the methods mentioned above use additional attachments to the section. These methods are effective and appropriate when the existing bridges don't have sufficient aerodynamic stability.

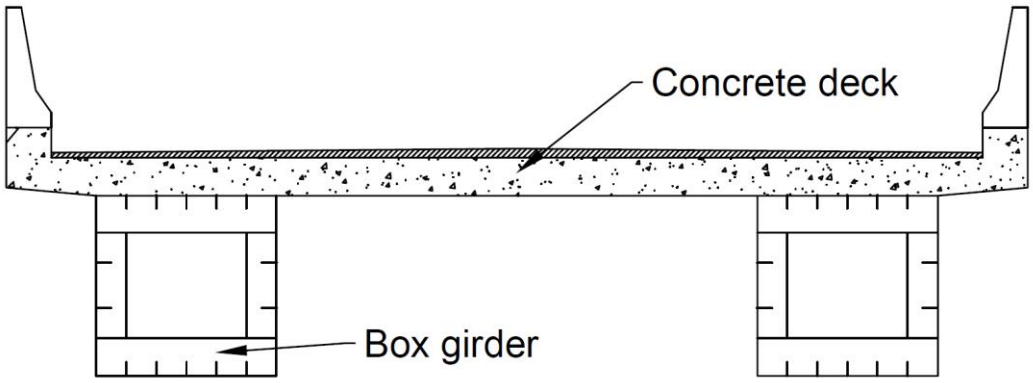

Fig. 1 Typical shape of 2-edge box girder

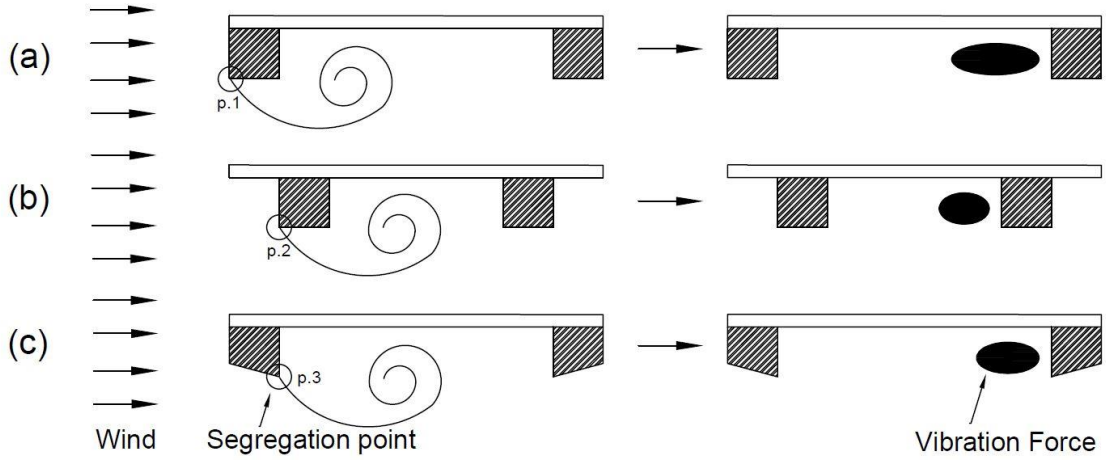

Fig. 2 Vortex and vibration generating mechanism for 2-edge box girder

Alternatively, aerodynamic stability can be increased by using a stabilized section (Daito 2004). Daito designed a steel box with a slope, as shown in Fig. 2(c). By providing a slope to the box section, the vibration force can be reduced compared to the ordinary steel box girder section (the slope is equal to zero for an ordinary steel box girder section), as shown in Fig. 2 (Daito 2004).

For a rectangular box, the segregation point (vortex starting point) is located in P1 as shown in Fig. 2(a). By decreasing the distance between the boxes, the vibration force can be reduced, as shown in Fig. 2(b). However, this method is not appropriate, since the torsional stiffness of the whole bridge can be significantly affected by the distance between the two boxes. Also, the reduced distance between the two boxes can result in poor torsional stiffness of the system. When the specific slope range is applied to the box, as shown in Fig. 2(c), the segregation point may move from P1 to P3 and the vibration force can be reduced compared to the case shown in Fig. 2(a). This increased aerodynamic stability is the basic idea of the stabilized section. If the stabilized section is properly considered in the initial design of the bridge section, the aerodynamic stability can be increased without the additional attachment after the construction of the bridge.

Some researchers (Daito 2004) have studied Vortex Induced Vibration (VIV) and flutter stability for stabilized sections, as shown in Fig. 2(c), demonstrating the excellent VIV and flutter stability performances of the stabilized section. However, their studies are limited to the dynamic stability of the stabilized section, even though the aerodynamic static response of the bridge is as important as the dynamic response. The static aerodynamic coefficients are essential parameters for evaluating the wind resistance of a bridge.

This study focuses on the evaluation of the static aerodynamic response of the stabilized section. For this study, box slopes were varied from 0° to 17° and static coefficients were obtained through a series of wind tunnel tests. In generally, static coefficients are depended on Reynolds number. So, Reynolds number test was also conducted because static coefficients can be had remarkably difference value for certain Reynolds number range. The results were then compared with those from the CFD analysis. From the results, it was found that the drag coefficients generally decreased with the increasing box slope angle, except the specific ranges of the box slope. This range is varied depending on the B/H ratio of the section, where B and H are the width and height of the section, respectively.

2. Wind tunnel test

2.1 Section description

Fig. 3 shows the 2-edge box girder bridge section considered in this study. The target bridge has a span of approximately 700 m with 4 lanes. The stiffened girder has a composite section, as shown in Fig. 3. The width, B, and height, H, of the bridge section are 34.0 m and 3.7 m, respectively. Thus, the B/H ratio is approximately 9.2. The width of the box is 4.8 m and the outer height of the box is 1.9 m. The inner box height is 3.4 m and this results in a box slope of 17°, as shown in Fig. 3. It should be noted that the B/H of the stiffened girder generally varies from 5 to 12.5 (Daito *et al.* 2002). The target section of this study has a B/H of 9.2, which is the average B/H ratio of the stiffened girder.

A 1:70 scale model was fabricated for the wind tunnel test. The detail dimensions of the model for the wind tunnel test are shown in Table 1. The surface of the test model was fabricated as smooth as possible so that the effect of surface roughness is negligible. Also, the test model was

made to have sufficient rigidity so that no deformation of the model would occur during the wind tunnel test. To satisfy these characteristics, the test model was made by using Acrylonitrile Butadiene Styrene (ABS) and Foamex materials.

The scaled model was designed to have the same center of mass and moment as those of the original section. The experiment pathway blockage ratio was controlled to be less than 5%.

Table 1 Details of test section

Character	Value
Scale	70:1
Width	0.485 m
Length	1.000 m
Height	0.053 m

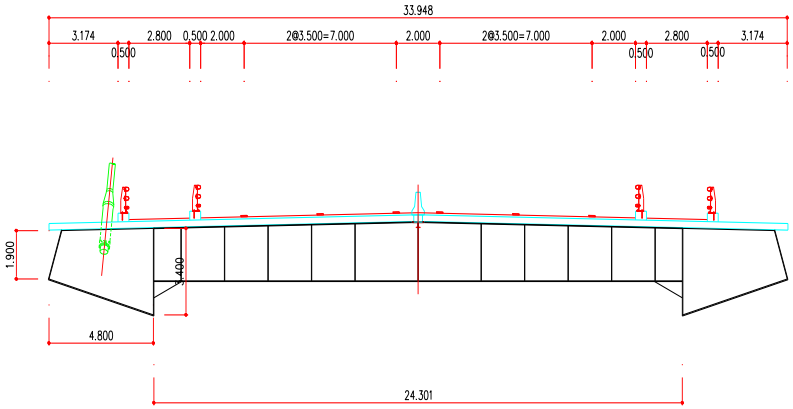

Fig. 3 Target section

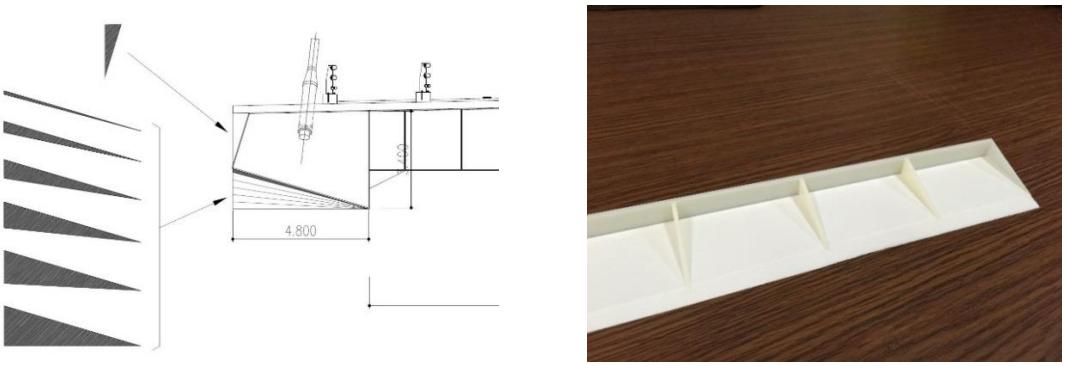

(a) Slope variation with various attachment brackets (b) Attachment bracket

Fig. 4 Test section

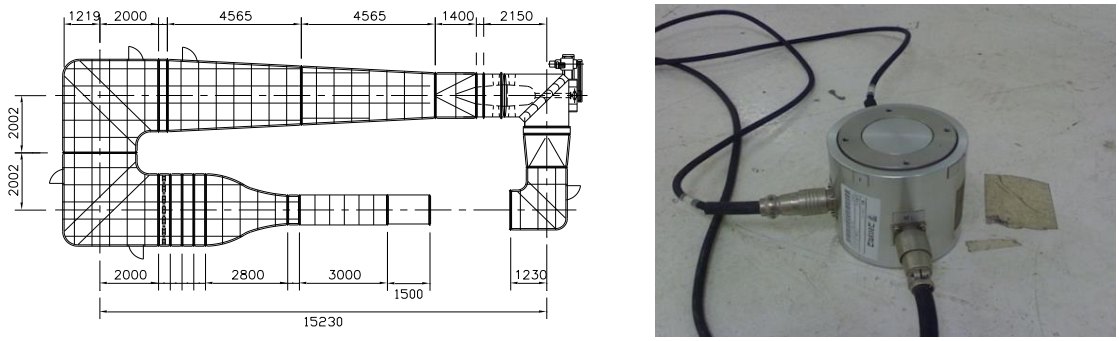

(a) Layout of wind tunnel (b) Load cell (LMC-3501-5, Nissho)

Fig. 5 Wind tunnel test facilities

2.2 Wind tunnel test setting and parameters

The test was performed in the Wind Tunnel Laboratory at Korea University. The layout of the wind tunnel used in this study is shown in Fig. 5(a). The dimensions of inlet part by the test section are 1.0 m x 0.8 m x 1.5 m (Width x Height x Length). 3-component load cells (LMC-3501-5, Nissho) were used to obtain the 3-dimensional aerodynamic forces, as shown in Fig. 5(b). The static aerodynamic force coefficients can be obtained from

$$F_d = \frac{1}{2}\rho U^2 B C_d \tag{1}$$

$$F_l = \frac{1}{2}\rho U^2 B C_l \tag{2}$$

$$F_m = \frac{1}{2}\rho U^2 B^2 C_m \tag{3}$$

where F_d is the drag force, F_l is the lift force, F_m is the moment force in the model, ρ is the density of air, U is the velocity, B is the deck width, C_d is the aerodynamic drag force coefficient, C_l is the aerodynamic lift force coefficient, and C_m is the aerodynamic moment force coefficient.

(a) Side view (b) Front view

Fig. 6 Example of test setup (box slope angle = 9°)

Table 2 Wind tunnel test cases

No.	List	Flow	Slope angle	Wind speed	Reynolds number	Step
1			0°			
2			3°			
3			6°			
4	C_d, C_l, C_m	Uniform	9°	0 ~ 10 m/s	0 ~ 3.5x10^5	30
5			12°			
6			15°			
7			17°			

Fig. 6 shows an example of the test setup, where the box slope angle is equal to 9°. The same test setup was applied to all other cases.

Wind tunnel tests to evaluate the static aerodynamic coefficients (C_d, C_l, and C_m) were conducted for various box angle slopes. The box slope angles considered were 0°, 3°, 6°, 9°, 12°, 15°, and 17°, as shown in Table 2. The air flow was uniform and the wind speed varied from 0 to 10 m/s. Reynolds numbers ranged from 0 to 3.5 x 10^5.

The variation of static aerodynamic coefficients with Reynolds number is discussed in this section. Reynolds number is defined as

$$Re = \frac{UD}{\nu} \tag{4}$$

where Re is the Reynolds number, D is the reference length, and ν is the kinematic viscosity. In this study, D is set as 0.4857(≒34.0/70) m based on the target section shown in Fig. 3 and ν is 15.1 x 10^{-6} m^2/s. For each test, Re was obtained based on Eq. (4) and the aerodynamic coefficients (C_d, C_l, and C_m) were evaluated by using the relationship between aerodynamic forces and the aerodynamic coefficients (Eqs. (1)-(3)).

2.3 Test result

2.3.1 Variation of static coefficients with Reynolds number

The test results for C_d, C_m, and C_l are shown in Figs 7-9, respectively. It was found that the C_d value decreased with the increasing slope angle, as shown in Fig. 7, except for the case with the slope angle of 9°. The C_d value for the box slope of 9° was similar than that of the case having a slope angle of 3°. This implies that the static drag force can be suddenly increased for a certain box slope (9° in this case) and C_d does not simply decrease with the increasing box slope angle.

Fig. 8 shows the relationship between C_m and the Reynolds number for various box slope angles. C_m was almost equal to zero. Among the various C_m, values, that for the box slope of 9° was the farthest from zero and showed the poorest static aerodynamic response. The test results for C_l are shown in Fig 9. In the case of C_l, it was observed that the special relationship between the Reynolds number and C_l did not depend on the box slope.

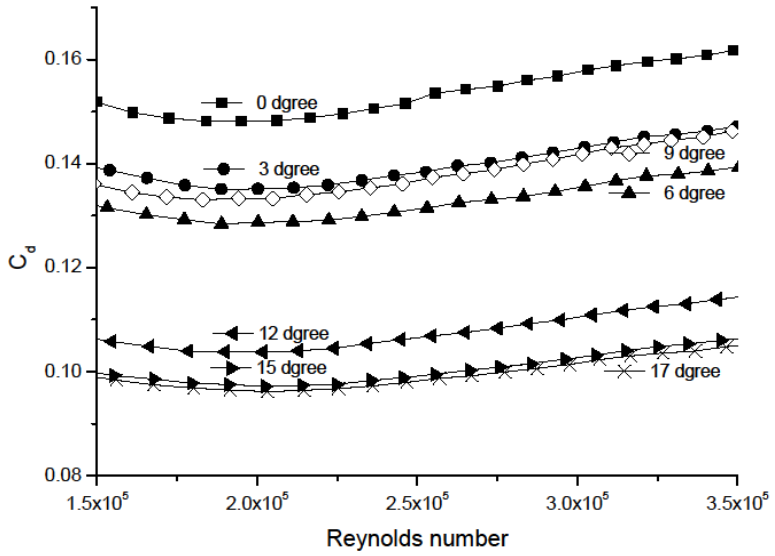

Fig. 7 C_d vs. Reynolds number for various box slope angles

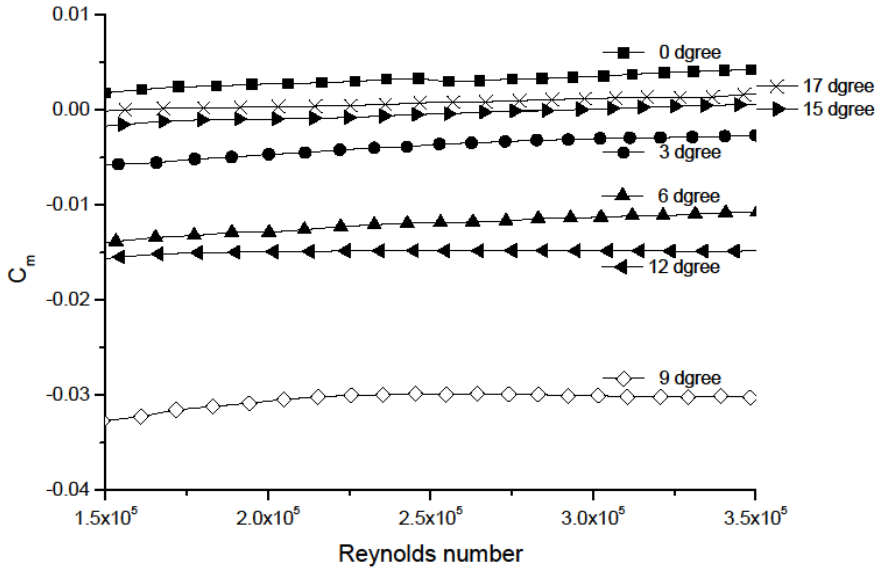

Fig. 8 C_m vs. Reynolds number for various box slope angles

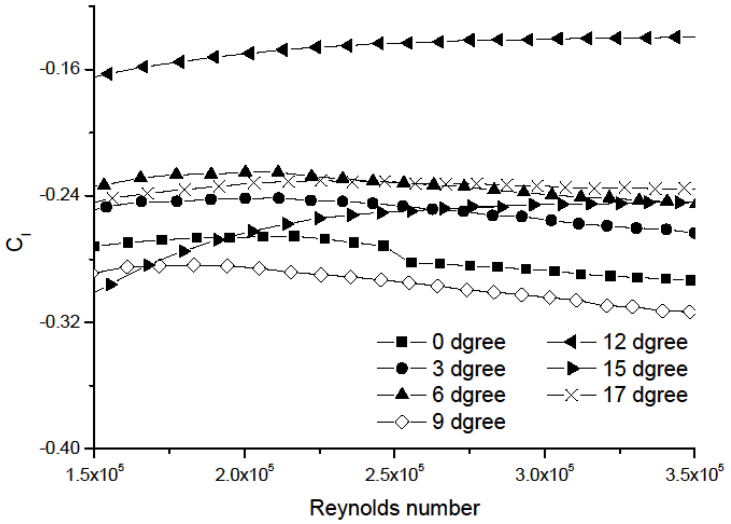

Fig. 9 C_l vs. Reynolds number for various box slope angles

2.3.2 Variation of static coefficients with slope angle

The relationship between C_d and the box slope angle is shown in Fig. 10 for a wind speed of 5.2 m/s and 10.2 m/s, respectively. From Fig. 10, it can be seen that C_d decreased with the increasing slope angle, except for the box slope of 9°. For the box slope angle of 9°, C_d suddenly increased. Similar behavior was noted for all wind speed ranges considered in this study (from 5 m/s to 10 m/s).

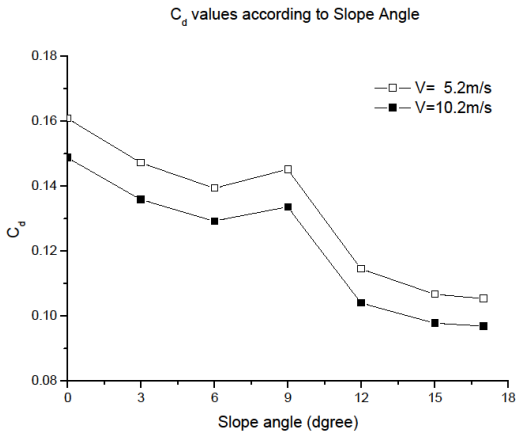

Fig. 10 Variation of C_d with box slope angle

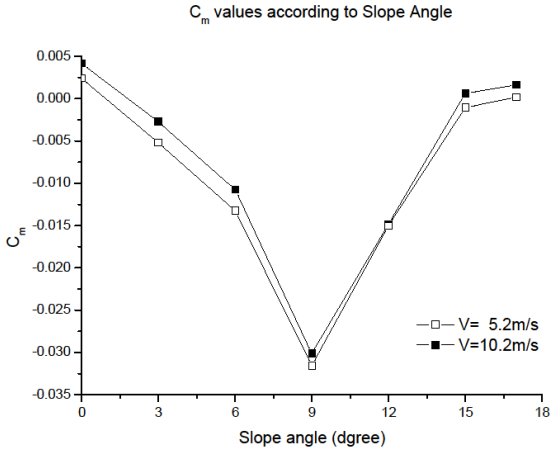

Fig. 11 Variation of C_m with box slope angle

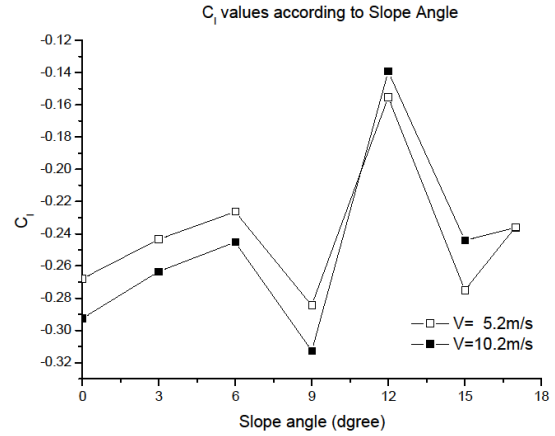

Fig. 12 Variation of C_l with box slope angle

Fig. 11 shows the relationship between C_m and the box slope angle. It was found that the C_m decreased with the increasing box slope angle up to the box slope of 9°. C_m had the minimum value when the box slope angle was equal to 9°. Thereafter, C_m increased with the increasing box slope angle. The static aerodynamic response is the poorest for the case having the box slope angle of 9°. However, C_m was very small compared with C_d and C_l. Thus, C_m is not a governing parameter when evaluating the static aerodynamic response of this section. A similar phenomenon was observed for all wind speeds considered in this study. The relationship between C_l and the box slope angle is shown in Fig. 12. It was found that the C_l value does not have a special relationship with the slope angle.

In summary, it can be seen that C_d, C_m, and C_l are not simply proportional to the box slope angle. For the box slope angle of 9°, C_d and C_m are the worst. To more closely investigate this phenomenon, CFD analysis was performed. The details of the analysis are shown in the following section.

3. CFD analysis

3.1 Analysis model description

The CFD analysis was conducted for the test section herein. The CFD analysis condition is shown in Table 3. A 1:70 scale model was used for the simulations. For unsteady simulations, the incompressible turbulent flow around the 2D analyzed sections was modeled by using the classical Navier-Stokes equations. In the simulations, the Reynolds Averaged Navier-Stokes (RANS) equation was employed: realizable κ-ε model with enhanced wall treatment.

The turbulent characteristics of the flow was defined in terms of intensity (0.1%) and length scale (0.485 m). The Finite Volume solver, Fluent, by ANSYS (ANSYS, 2016) was used to numerically evaluate the flow field. A quadrilateral mesh using the Quad scheme of the flow domain was employed. The total number of cells in the computational grids was approximately 400,000. Simulations were carried out for Reynolds numbers $2.7x10^5$ based on the width of section. Advancement in time is accomplished by using a second-order implicit scheme, and a Pressure Implicit with Splitting of Operator (PISO) algorithm was used for the pressure-velocity coupling. The time step was equal to 0.001 and the number of iterations per time step was 20. The unsteady simulations were performed until a periodic behavior was reached (Latif Attia and Aziz Ahmed 2016).

Table 3 CFD analysis conditions

Note	Condition
Section Scale	1:70
Dimension	2D
Number of Grid	≒400,000
Equation	Navier-stokes Eqn.
Turbulence Model	Realizable (κ-ε) with enhanced wall treatment
Wall Function	Non slip
Range of y+	5 < y+ < 10
Wind Velocity	8 m/s
Reynolds number	$2.7x10^5$

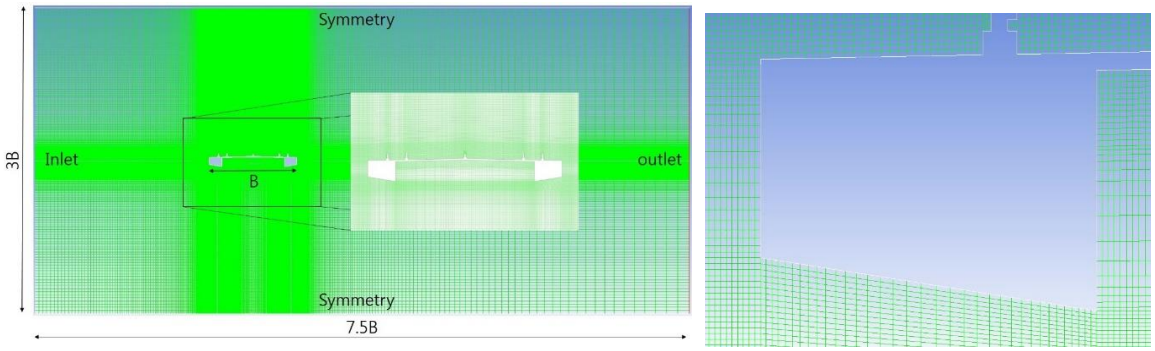

Fig. 13 Analytical domain and boundary conditions (box slope angle of 9°)

Fig. 13 shows the analytical domain and boundary conditions used in this study. The boundary conditions of the left end were set on the inlet plane as the boundary of inflow U. The non-slip boundary condition is set on the surface of the box girder section. The boundary condition of the advection type is introduced on the outlet plane. The dimensionless wall distance was set as 5<y+<10 (Watanabe and Fumoto 2008, Salim and Cheah 2009).

CFD analyses were conducted for the box slope angles of 0°, 3°, 6°, 9°, 12°, 15, and 18°. The results were then compared with the wind tunnel test results for verification purpose. From the wind tunnel test, the case having the box slope of 9° shows the poorest static aerodynamic behavior compared to the other cases. Thus, an additional analysis near 9° was conducted (for 7°, 8°, 10°, and 11°).

3.2 Analysis model verification

The static aerodynamic coefficients were obtained from the CFD analysis and the results were compared with the wind tunnel test results. Comparison results for C_d and C_l are shown in Fig. 14.

In Fig. 14, it can be seen that the trend of C_d and C_l from CFD analysis is similar to that obtained from the wind tunnel test. The maximum discrepancy between CFD analysis and the wind tunnel test was 13% and 17%, respectively.

From the analysis results, C_d suddenly increased for the box slope range from 8° to 11°. To find the reason of this phenomenon, the Turbulent Kinetic Energy (TKE), stream line, and pressures were analyzed. The details are discussed in the following section.

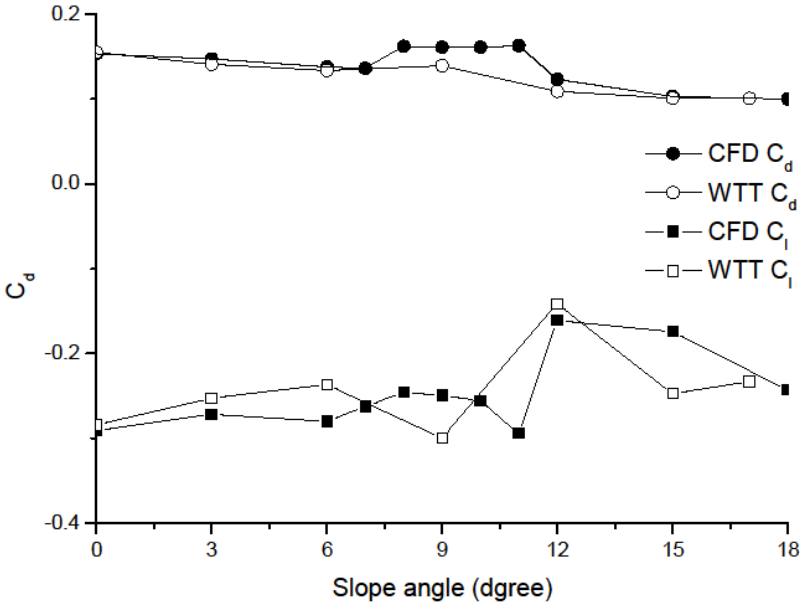

Fig. 14 Comparison of C_d and C_l from CFD with those from WTT

3.3 CFD analysis result (TKE, Streamline, Pressure)

The TKE was calculated for each model. Figs. 15(a)-15(c) show the TKE for the box slopes of 3°, 9°, and 18°, respectively. It should be noted that C_d suddenly increases when the box slope is equal to 9° and C_d has a minimum value when the box slope is 18°.

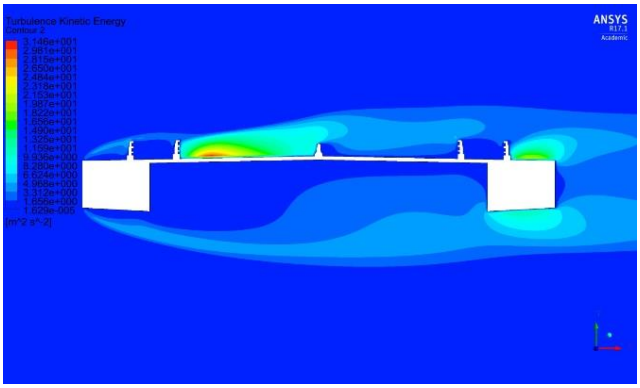

(a) TKE for box slope angle 3°

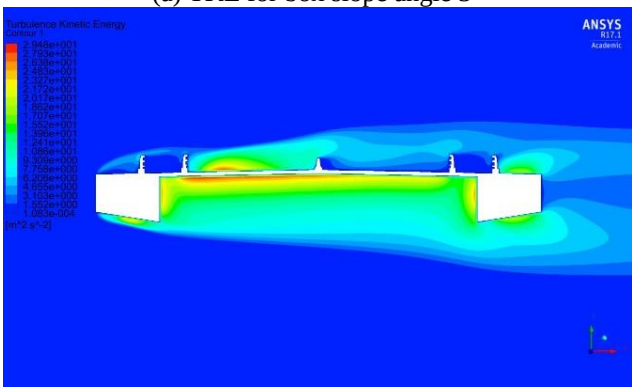

(b) TKE for box slope angle 9°

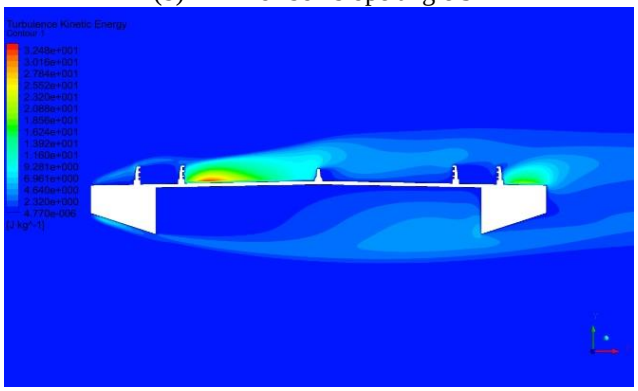

(c) TKE for box slope angle 18°

Fig. 15 Comparison of TKEs

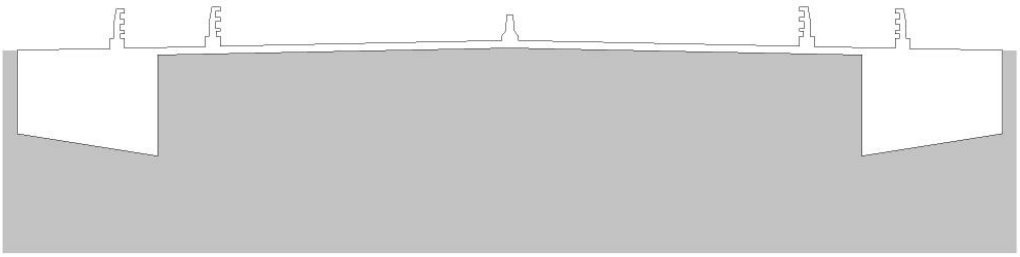

Fig. 16 Boundary for the total sum of TKE

Fig. 15(a) clearly shows that a large TKE is generated in the lower part of the cross-section when the box slope is equal to 9°. Similar TKE distribution can be observed for the box slope range of 8°-11°. On the other hand, TKE is considerably reduced for the box slopes of 3° and 18°. Thus, it can be seen that C_d is related to the TKE distribution.

For each analysis model, the total sum of TKE was calculated based on the rectangular box shown in Fig. 16, where the width and height of the box is 0.5 m and 0.1 m, respectively.

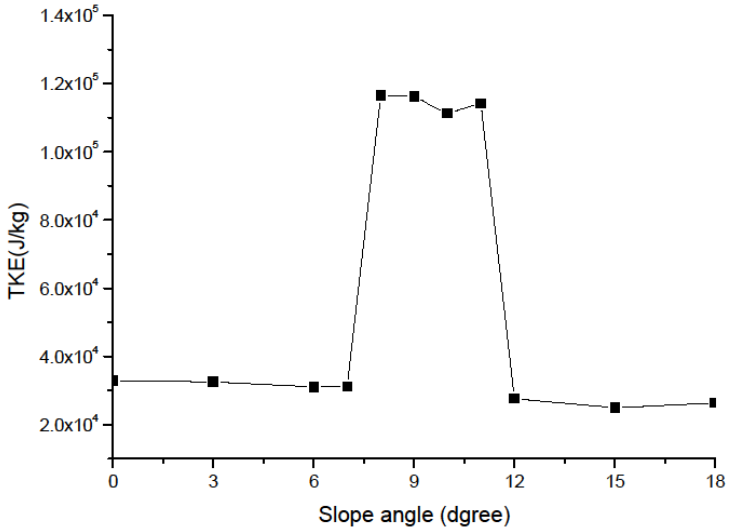

Fig. 17 TKE vs. slope angle from CFD analysis

The relationship between TKE and the slope angle is shown in Fig. 17. It can be seen that the TKE suddenly jumped for the box slope range of 8°-11°. This phenomenon is fairly similar to the relationship between C_d and the box slope.

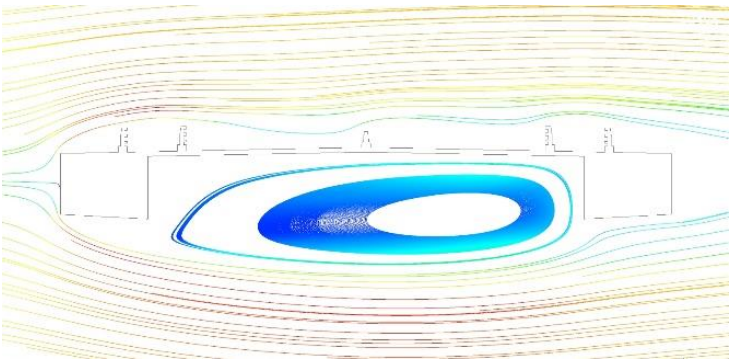

(a) Stream line for box slope angle 3°

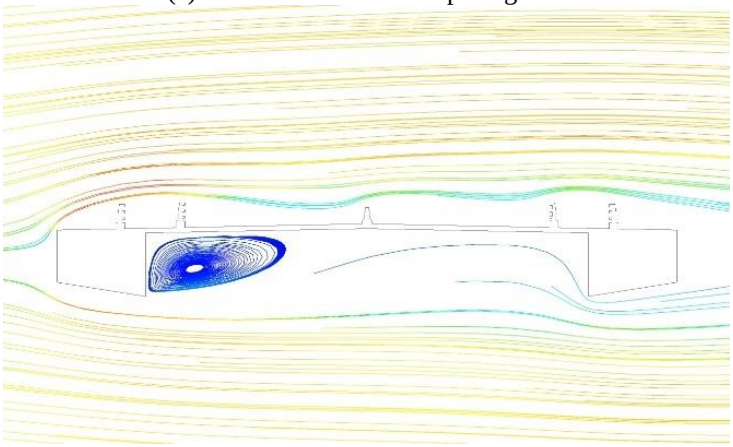

(b) Stream line for box slope angle 9°

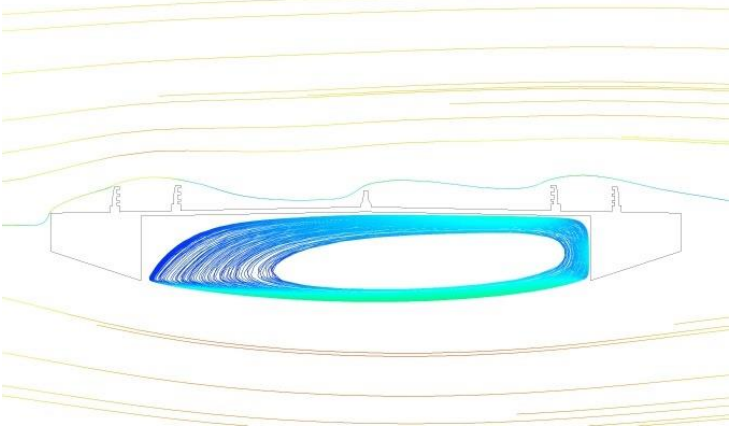

(c) Steam line for box slope angle 18°

Fig. 18 Comparison of stream lines

Figs. 18(a)-18(c) show the stream lines for box slope angles of 3°, 9°, and 18°, respectively. The vortex separation point changes depending on the box slope. The vortex patterns then changed as shown Fig. 18 (Fransos and Bruno 2010). The type and pattern of the vortex affect the bridge deck (Larsen and Wall 2012). In Fig. 18(b), it can be seen that a localized vortex is generated near the left box when the box slope angle is 9°. Thus, air pressure is applied on the windward box (left box) first. Then, the secondary air pressure acts on the leeward box (right box). A similar stream line was observed for the case with the box slope angle of 8°-11°. In this box slope region, the TKE and C_d values are comparatively large.

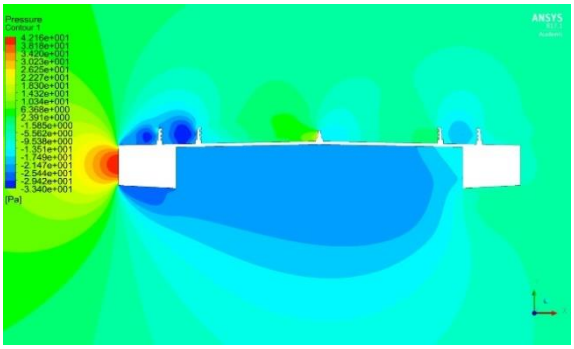

(a) Pressure contour for box slope angle 3°

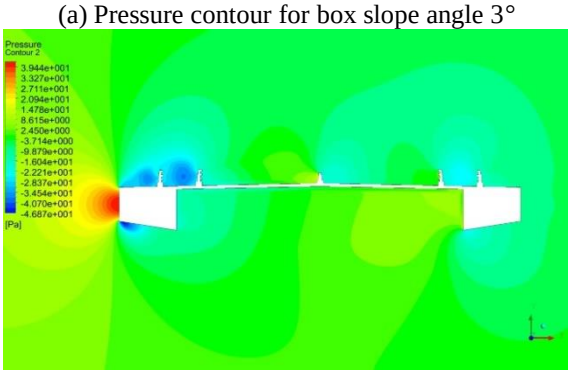

(b) Pressure contour for box slope angle 9°

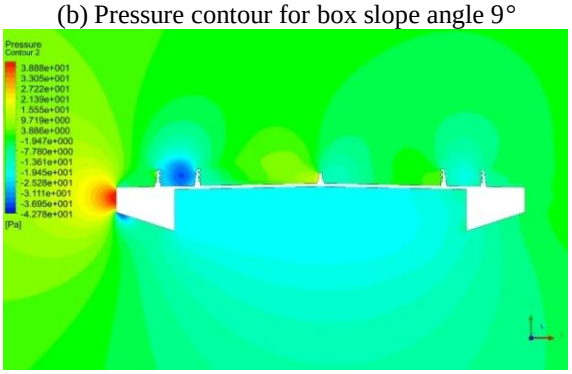

(c) Pressure contour for box slope angle 18°

Fig. 19 Comparison of pressure contours

On the other hand, for the box slope angles of 3° and 18°, a vortex is generated in the space between the windward and leeward box, as shown in Figs. 18(a) and 18(c). Due to the interaction between the wind and deck shape, a recirculation zone is formed and the stream line around the bridge is quite similar to that of the single box girder (Vaz *et al.* 2016). From the stream line analysis results, it can be seen that the stream line shape changes depending on the box slope angle. When the box slope ranges from 8° to 11°, the vortex is localized and a secondary impact acts on the girder. This increases the TKE and C_d values. And this phenomenon affects only drag force without lift and moment force. It cannot be seen a special relationship with C_l values and the slope angle, also C_m values.

To clarify this phenomenon, the pressure forces acting on the windward and leeward box were visualized. Pressure distribution is one of the parameters used in the evaluation of the aerodynamic characteristics of a bridge deck (Ricciardelli and Hangan 2001). Pressure contours for the box slope angles of 3°, 9°, and 18° are shown in Figs. 19(a)-19(c), respectively. Furthermore, the pressure forces acting on the left section of the windward box and leeward box are presented as a bar chart for the box slopes of 3°, 9°, and 18° in Figs. 20(a)-20(c), respectively.

It can be seen that both pressure forces acting on the windward and leeward box had positive values for the case with the box slope angle of 9°. On the other hand, for the box slope angles of 3° and 18°, the pressure forces on the windward and leeward box have different directions. This means that the girder tends to move from left to right when the box slope angle is 9° and from right to left when the box slopes are 3° and 18°.

To quantify the pressure forces acting on the girder, the average wind pressure force acting on the left side of the windward and leeward boxes were calculated as shown in Fig. 21. In Fig. 21, it can be seen that, for the windward box, the variation of average wind pressure force decreases with the increasing box slope angle. However, for the leeward box, the average wind pressure forces suddenly jumped for the box slope angle of 8°-11°. As mentioned previously, the localized vortex has a secondary impact on the leeward box, which increases the TKE and wind pressure forces. As a result, the C_d values are comparatively large for the box slope angle of 8°-11°.

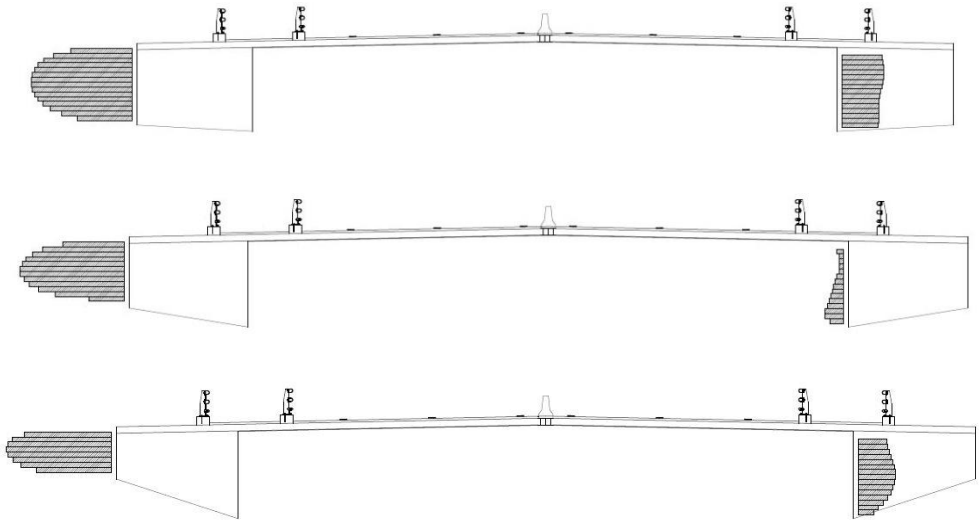

Fig. 20 Pressure diagram for slope angle 3° (Up) & slope angle 9° (middle) & slope angle 18° (bottom)

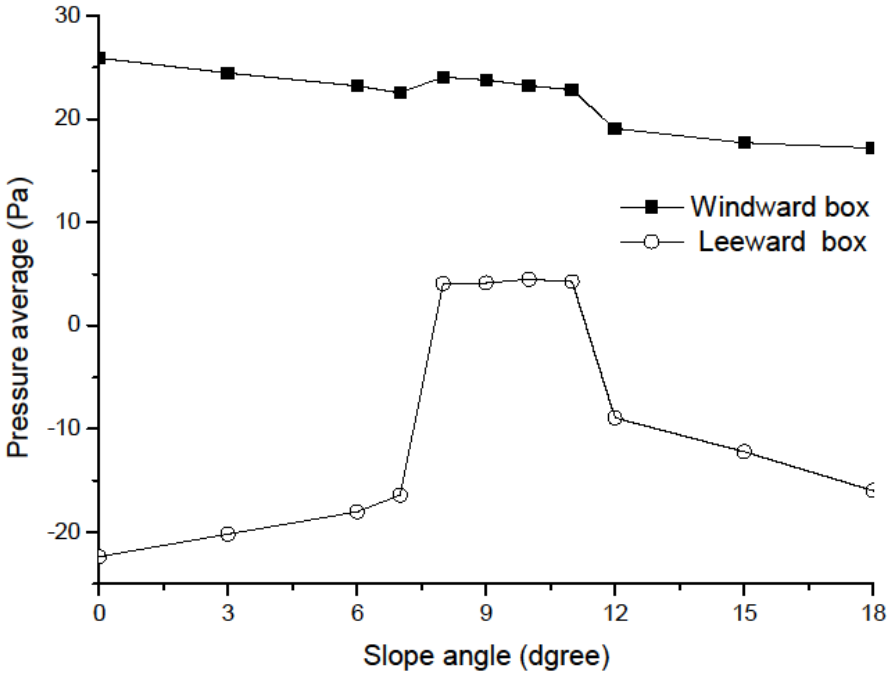

Fig. 21 Pressure vs. box slope angle

To cover a practical range of the B/H ratio, an additional parametric study was conducted. Two further sets of simulation were carried out. The B/H ratios of the first and second cases are 6.7 and 11.7, respectively. To change the B/H ratio, the inner box height was controlled. The width, B, and height, H, of the bridge section and the width of the box are the same as those of the original section. CFD analyses were conducted for the box slope angles of 0°, 3°, 6°, 9°, 12°, 15, and 18° for two cases.

From the first case of the CFD result, the phenomenon of the secondary impact acting on the girder could not be found for any box slope angle. From the second case of the CFD result, this phenomenon was found for the box slope range of 3°-24°. This result suggests that the box slope range occurring due to this phenomenon is expended by increasing the B/H ratio.

4. Conclusions

In this study, to overcome the weak aerodynamic stability of the 2-edge box girder section, the slope box concept (stabilized section) was introduced. The focus was made on the static aerodynamic response of the stabilized section. The major findings of this study are as follows.

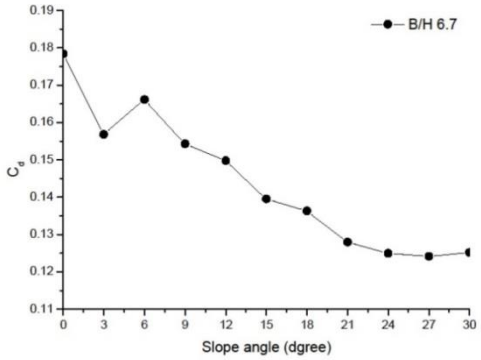

(a) C_d for slope angle at B/H ratio 6.7

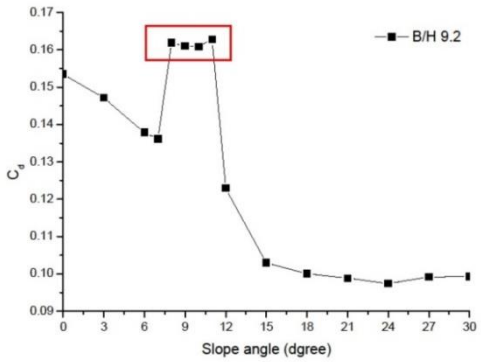

(b) C_d for slope angle at B/H ratio 9.2 (original section)

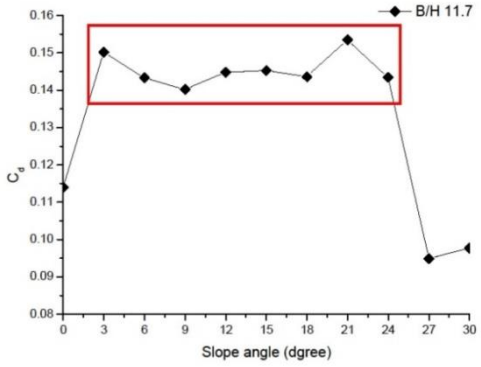

(c) C_d for slope angle at B/H ratio 11.7

Fig. 22 C_d vs. box slope angle by B/H ratio

From the wind tunnel test results, it can be found that the static drag force can suddenly increase for a certain box slope (9°) and C_d does not simply decrease with the increasing box slope angle. To investigate this phenomenon in more detail, CFD analysis was performed for the test model. From the CFD analysis, the general trend of C_d obtained from CFD analysis is similar to that from the wind tunnel test. Also, it was found that the TKE suddenly jumps for the specific box slope range (8°-11°) and this phenomenon is fairly similar to the relationship between C_d and the box slope. From stream line analysis, it can be seen that the localized vortex is generated near the left box for the same specific box angle. Then, the secondary air pressure acts on the leeward box (right box). For this specific box angle, both pressure forces acting on the windward and leeward boxes had a positive value. It should be noted that this phenomenon is not directly related to the lift and moment force. Thus, a correlation between C_l and C_m and the box slope were not found.

Finally, the parametric study was conducted for various B/H ratio of the target section (B/H=6.7, 9.2, and 11.7). From the results, it was founded that the box slope range, that induce the secondary impact by the vortex, is expended by increasing B/H ratio.

References

ANSYS Inc. (2016), ANSYS Fluent User's Guide, Release 17.1.

Bruno, L., Khris, S. and Marcillat, J. (2001), "Numerical simulation of the effect of section details and partial streamlining on the aerodynamics of bridge decks", *Wind Struct.*, **4**(4), 315-332.

Daito, Y., Matsumoto, M. and Araki, K. (2002), "Torsional flutter mechanism of two-edge girders for long-span cable-stayed bridge", *J. Wind. Eng. Ind. Aerod.*, **90**, 2127-2141.

Daito, Y., Matsumoto, M. and Takeuchi, T. (2004), "Aerodynamic stabilization for geometrical girder shape of tow edge girder of long span cable stayed bridges", *Proceedings of the 18th National Symposium on Wind Engineering*, Tokyo, Japan, July.

Fransos, D. and Bruno, L. (2010), "Edge degree-of-sharpness and free-stream turbulence scale effects on the aerodynamics of a bridge deck", *J. Wind. Eng. Ind. Aerod.*, **98**, 661-671.

Haque, M.N., Katsuchi, H., Yamada, H. and Nishio, M. (2016), "Investigation of edge fairing shaping effects on aerodynamic response of long-span bridge deck by unsteady RANS", *Arch. Civil Mech. Eng.*, **16**, 888-900.

Ito, M. (1996) "Cable-supported steel bridges: design problem and solutions", *J. Construct. Steel Res.*, **39**(1), 69-84.

Larsen, A. and Wall, A. (2012), "Shaping of bridge box girders to avoid vortex shedding response", *J. Wind. Eng. Ind. Aerod.*, **104-106**, 156-165.

Latif Attia, W.A. and Aziz Ahmed, A.A. (2016), "Aeroelastic Investigation of Long Span Suspension Bridge Decks by Numerical CFD and FSI Analyses", *Civil Environ.Res.*, **8(7)**, 81-90.

Matsumoto, M., Shirato, H. and Yagi, T. (2000), "Recent topics on bridge aerodynamics", *Wind Struct.*. **3**(4), 267-277.

Miyata, T. (2003), "Historical view of long-span bridge aerodynamics", *J. Wind. Eng. Ind. Aerod.*, **91**, 1393-1410.

Mstsumoto, M., Nakajima, N., Taniwaki, Y. and Shijo, R. (2001), "Grating effect on flutter instability", *J. Wind. Eng. Ind. Aerod.*, **89**, 1487-1497.

Ricciardelli, F. and Hangan, H. (2001), "Pressure distribution and aerodynamic forces on stationary box bridge sections", *Wind Struct.*, **4**(5), 399-412.

Sakai, Y., Ogawa, K., Shimodoi, H. and Saitoh, T. (1993), "An experimental study on aerodynamic improvements for edge girder bridge", *J. Wind. Eng. Ind. Aerod.*, **49**, 459-466.

Salim, S.M. and Cheah, S.C. (2009), "Wall y+ strategy for dealing with wall-bounded turbulent flows", *Proceedings of the International MultiConference of Engineers and Computer Scientists*, Hong Kong,

March.
Simiu, E. and Scanlan, R.H. (1996), *Wind Effects on Structures*, 3rd Ed., John Wiley and Sons, Inc.
Vaz, D.C., Almeida, R.A.B., Didier, E., Urgueira, A.P.V. and Borges, A.R. Janeiro (2016), "Improving the aerodynamic performance of Vila-Real Bridge deck-section", *J. Wind. Eng. Ind. Aerod.*, **156**, 72-83.
Watanabe, S. and Fumoto, K. (2008), "Aerodynamic study of slotted box girder using computational fluid dynamics", *J. Wind. Eng. Ind. Aerod.*, **96**, 1885-1894.

CC